Cell Reports
Physical Science

CellPress
OPEN ACCESS

Article

Photo-induced catalytic C—H heteroarylation of group 8 metallocenes

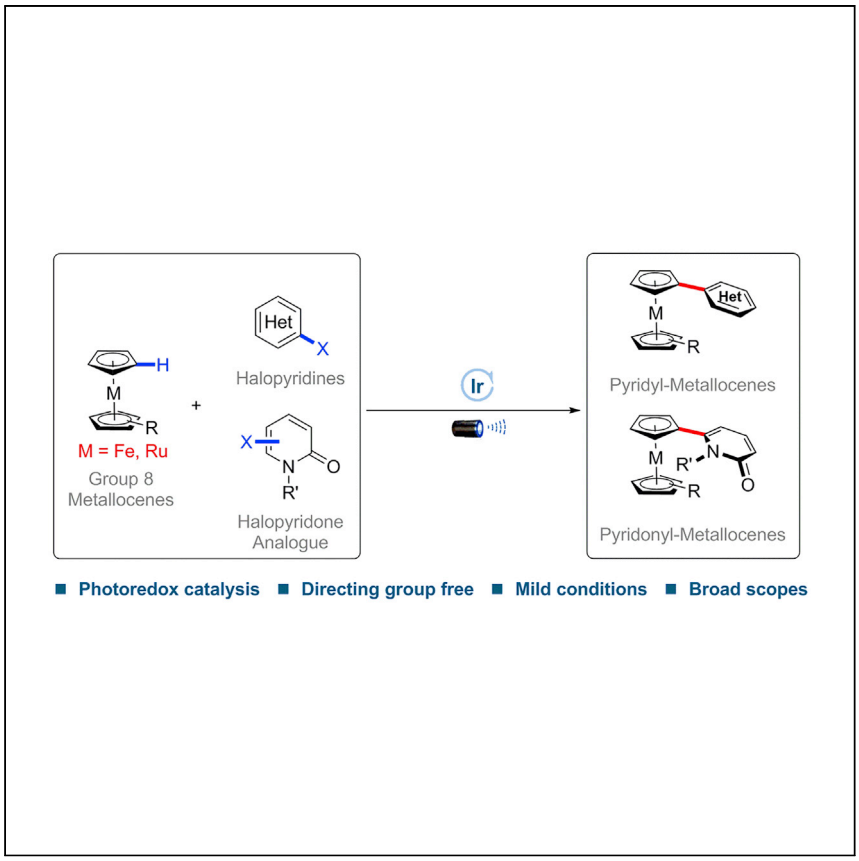

Metallocenes and their derivatives play an important role in materials science, medicinal chemistry, and catalysis. Here, He et al. describe a photo-induced catalytic C—H heteroarylation of ferrocenes and ruthenocenes with aryl halides to access pyridyl and pyridonyl metallocenes.

Gu-Cheng He, Shi-Yu Guo, Hao Zheng, ..., Xiang-Ting Min, Ding-Wei Ji, Qing-An Chen

qachen@dicp.ac.cn

Highlights

Photoredox heteroarylation of group 8 metallocenes without directing group

Intermolecular radical cross coupling under mild conditions

Further synthetic transformation of pyridyl ferrocenes

He et al., Cell Reports Physical Science 3, 100768
February 16, 2022
https://doi.org/10.1016/j.xcrp.2022.100768

Cell Reports
Physical Science

CellPress
OPEN ACCESS

Article

Photo-induced catalytic C−H heteroarylation of group 8 metallocenes

Gu-Cheng He,[1,2,3] Shi-Yu Guo,[1,3] Hao Zheng,[1,2] Chang-Hui Liu,[1,2] Ying Li,[1,2] Xiang-Ting Min,[1] Ding-Wei Ji,[1] and Qing-An Chen[1,2,4,*]

SUMMARY

Possessing a characteristic sandwich-type structure, metallocenes have been widely used by the chemistry community. However, the direct catalytic C−H heteroarylation of metallocenes still remains underexplored. Here, we report an efficient catalytic protocol for C−H heteroarylation of group 8 metallocenes (M = Fe, Ru) under light irradiation. This intermolecular cross coupling features directing group free, mild conditions and a wide substrate scope. Preliminary mechanistic studies suggest that the newly formed C−C bond is constructed through electrophilic radical substitution of the metallocene with a heteroaryl radical, which is generated via an oxidative quenching pathway.

INTRODUCTION

Ferrocenes,[1–3] a class of important and prevalent metallocenes, have gained much attention owing to their unique structure and excellent performance in materials science,[4–7] medicinal chemistry,[8–10] and catalysis.[11–15] Accordingly, new approaches for the functionalization of ferrocenes are of great significance in organic chemistry. Friedel-Crafts acylation and lithiation/nucleophilic reaction are two typical strategies for the functionalization of ferrocene.[16–20] As for (hetero)arylation of ferrocenes, the Negishi reaction is a reliable method for the multi-step synthesis of pyridyl ferrocenes, but a stoichiometric amount of pyrophoric *tert*-butyl lithium has to be used for the preparation of ferrocenyl zinc reagents (Figure 1A).[21] As a result, the direct catalytic C−H (hetero)arylation of ferrocenes is attractive but challenging.

Through catalytic C−H activation and a cross-coupling strategy, Pd-catalyzed intramolecular arylation of ferrocenes has been independently accomplished by You,[22] Gu, and Kang[23] (Figure 1B). In addition, with the assistance of preinstalled directing groups (DGs), You's group also realized the intermolecular C−H arylation of ferrocenes with aryl halides under Rh catalysis (Figure 1C).[24,25] These two distinct approaches both involve C−H activation at an elevated temperature.

Apart from transition metal catalysis, state-of-the-art photoredox catalysis[26–39] has pushed the boundary of catalytic arylation reactions using various aryl radical precursors.[40–44] However, for limited examples of photo-induced arylation of arenes or heteroarenes,[45–48] super stoichiometric substrates (>10 equivalent [equiv]) have to be used in order to guarantee acceptable yields in most cases. With respect to arylation of ferrocene, due to its unique structure, there are only a few reports that aryl ferrocenes could be achieved via Gomberg-Bachmann reaction with aryl diazo compounds (10 equiv).[49] Despite these impressive advances, photo-induced catalytic intermolecular C−H (hetero)arylation of metallocenes via a radical pathway still

[1]Dalian Institute of Chemical Physics, Chinese Academy of Sciences, Dalian 116023, People's Republic of China

[2]University of Chinese Academy of Sciences, Beijing 100049, People's Republic of China

[3]These authors contributed equally

[4]Lead contact

*Correspondence: qachen@dicp.ac.cn

https://doi.org/10.1016/j.xcrp.2022.100768

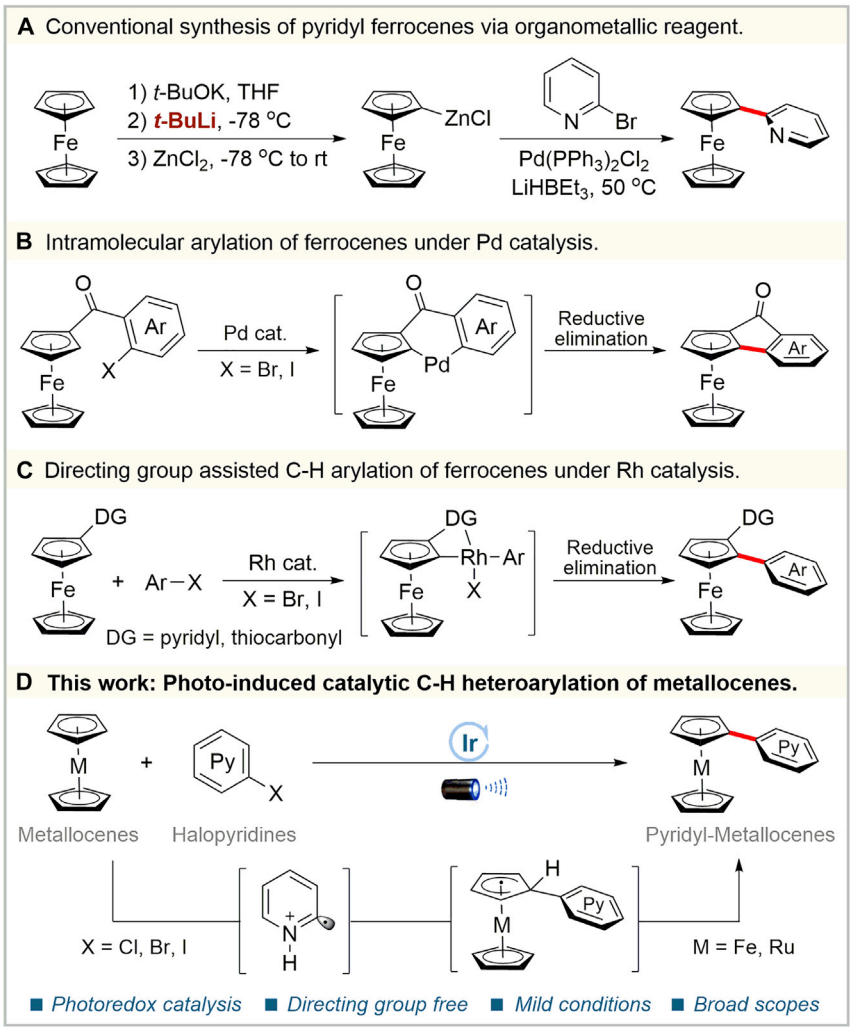

Figure 1. Arylation of group 8 metallocenes with aryl halides

(A) Conventional synthesis of pyridyl ferrocenes via organometallic reagent.

(B) Intramolecular arylation of ferrocenes under Pd catalysis.

(C) Directing-group-assisted C–H arylation of ferrocenes under Rh catalysis.

(D) This work: photo-induced catalytic C–H heteroarylation of metallocenes.

remains unknown. Inspired by the precedents about various pyridyl radical sources[50–56] and our work on photo-induced catalysis,[57–59] we report here a photo-induced catalytic C−H heteroarylation of ferrocenes and ruthenocenes with aryl halides (Figure 1D). This strategy features with broad substrate scope, mild and concise conditions, redox neutrality, elusions of DGs, and avoiding the use of flammable *tert*-butyl lithium reagent.

RESULTS AND DISCUSSION

Optimization

Initially, we aimed to optimize the reaction conditions of photo-induced pyridylation of ferrocene (Table 1). To assess the feasibility of our design, model substrates of ferrocene 1a and 2-bromo-6-methylpyridine 2a were examined under conditions that we recently developed for photo-induced halopyridylation of alkenes. A small amount of desired product 3a (19% yield) was obtained in the presence of

Table 1. Optimization for catalytic pyridylation of ferrocene

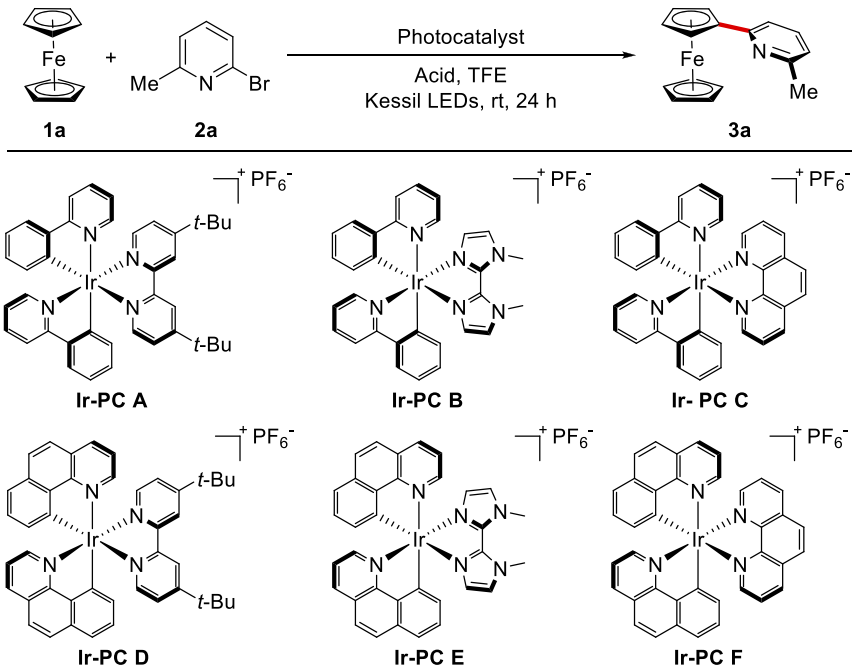

Entry[a]	PC	Acid	WL (nm)	Yield (%)[b]
1	Ir-PC A	TFA	456	19
2	Ir-PC A	TFA	427	30
3	Ir-PC A	TFA	390	43
4	Ir-PC A	TFA	CFL	trace
5	Ir-PC A	$PhCO_2H$	390	11
6	Ir-PC A	TsOH	390	11
7	Ir-PC A	$(PhO)_2PO_2H$	390	14
8	Ir-PC B	TFA	390	49
9	Ir-PC C	TFA	390	48
10	Ir-PC D	TFA	390	40
11	Ir-PC E	TFA	390	40
12	Ir-PC F	TFA	390	43
13	Ir-PC B	TFA	390	57[c]
14	Ir-PC B	TFA	390	76[c,d]
15	Ir-PC B	TFA	390	83[c,d,e]
16	Ir-PC B	TFA	–	ND
17	–	TFA	390	8
18	Ir-PC B	–	390	ND

WL, wavelength; PC, photocatalyst; CFL, compact fluorescent light; N.D., no detected; TFA, trifluoroacetic acid; TFE, 2,2,2-trifluoroethanol; TsOH, para-toluenesulfonic acid.

[a]Reaction conditions: 1a (0.30 mmol), 2a (0.20 mmol), photocatalyst (1.0 mol %), acid (2.0 equiv), TFE (2.0 mL), room temperature, under N_2, Kessil LEDs.

[b]Determined by GC-FID using mesitylene as the internal standard.

[c]TFE (4.0 mL).

[d]Ir-PC B (3.0 mol %).

[e]NaF (4.0 equiv) was added. Isolated yield was given.

$Ir(ppy)_2(dtbbpy)PF_6$ (Ir-PC A) at room temperature under the irradiation of blue LEDs (456 nm) (entry 1). Then, the evaluation on the wavelength of an LED suggested that 390 nm light was the optimal choice, making the yield increase to 43% (entries 1–3). The compact fluorescent light (CFL) only provided a trace amount of the desired

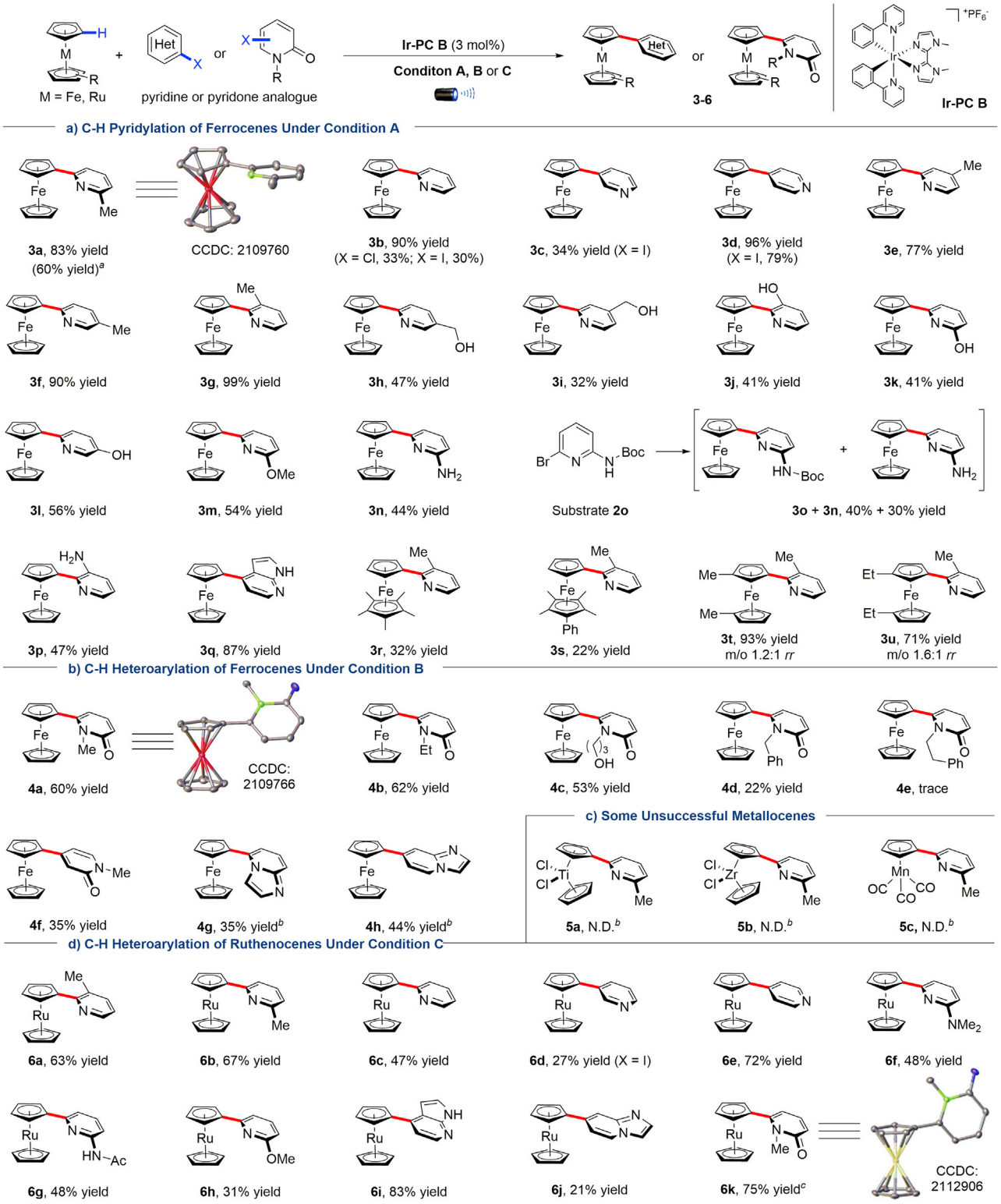
M = Fe, Ru
pyridine or pyridone analogue
Ir-PC B (3 mol%)
Conditon A, B or C
3-6
Ir-PC B
a) C-H Pyridylation of Ferrocenes Under Condition A
3a, 83% yield (60% yield)a
CCDC: 2109760
3b, 90% yield (X = Cl, 33%; X = I, 30%)
3c, 34% yield (X = I)
3d, 96% yield (X = I, 79%)
3e, 77% yield
3f, 90% yield
3g, 99% yield
3h, 47% yield
3i, 32% yield
3j, 41% yield
3k, 41% yield
3l, 56% yield
3m, 54% yield
3n, 44% yield
Substrate 2o
3o + 3n, 40% + 30% yield
3p, 47% yield
3q, 87% yield
3r, 32% yield
3s, 22% yield
3t, 93% yield m/o 1.2:1 rr
3u, 71% yield m/o 1.6:1 rr
b) C-H Heteroarylation of Ferrocenes Under Condition B
4a, 60% yield
CCDC: 2109766
4b, 62% yield
4c, 53% yield
4d, 22% yield
4e, trace
c) Some Unsuccessful Metallocenes
4f, 35% yield
4g, 35% yieldb
4h, 44% yieldb
5a, N.D.b
5b, N.D.b
5c, N.D.b
d) C-H Heteroarylation of Ruthenocenes Under Condition C
6a, 63% yield
6b, 67% yield
6c, 47% yield
6d, 27% yield (X = I)
6e, 72% yield
6f, 48% yield
6g, 48% yield
6h, 31% yield
6i, 83% yield
6j, 21% yield
6k, 75% yieldc
CCDC: 2112906

product (entry 4). Trifluoroacetic acid (TFA) kept its superior activation role compared with other Brønsted acids such as $PhCO_2H$, TsOH, and $(PhO)_2PO_2H$ (entries 5–7). Besides, the use of some widely used photocatalysts, such as (Arc-Mes)ClO_4, Rose Bengal, $Ru(bpy)_3Cl_2 \cdot 6H_2O$, and *fac*-$Ir(ppy)_3$, gave no better result than that of Ir-PC A (see Table S1). In order to further improve the product yield, several photocatalysts similar to Ir-PC A were synthesized and utilized for further optimization (entries 8–12). To our delight, Ir-PC B and C led to slight improvement on the yield, affording 49% and 48%, respectively (entries 8 and 9). A lower concentration could deliver a better result (57% yield), probably owing to the better light absorption (entry 13). Also, increasing the loading of Ir-PC B could further promote the reaction (entry 14). Finally, the addition of NaF gave the best isolated yield in 83% of the heteroarylation product 3a (entry 15). The role of NaF may help stabilize the protonized pyridyl radical by hydrogen bond interactions. Control experiments indicate that light irradiation, photocatalysts, and TFA are indispensable for the smooth formation of target product 3a (entries 16–18). A low yield of product was obtained without photocatalyst, probably because of the unique light absorption of ferrocene (entry 17).[60]

Substrate scope

With the optimized conditions in hand, we subsequently explored the pyridine substrate scope (Figure 2A). Subjecting 2a to the optimized condition afforded the target product 3a with 83% isolated yield. A 3.0 mmol scale-up reaction was conducted with 60% yield. The structure 3a was unambiguously confirmed by X-ray analysis with the dihedral angle of 17.4° between the Cp and pyridine rings. Beside 2-bromopyridine, Cl- and I-substituted pyridines could also deliver the target product (3b). Although C3-pyridylation produced lower yields (3c), good yields (79%–96%) were obtained for the C-4 pyridylation (3d). Alkyl-substituted pyridines showed good performance in the C-2 pyridylation (3e–3g). Hydroxymethyl groups on pyridines were also tolerated (3h–3i). Corresponding products were accessed with moderate yields with respect to pyridines bearing hydroxyl or methoxy groups (3j–3m). Slightly lower yields were obtained for primary amino group-substituted pyridines (3n and 3p). Beside normal product 3o, an *in situ* deprotection was observed for pyridine 2o. Delightfully, 4-bromo-1H-pyrrolo[2,3-*b*]pyridine furnished the biheterocyclic product with 87% yield (3q). For quinoline, isoquinoline halides, or benzene halides, this protocol did not work (see Scheme S1). Probably owing to the steric hindrance effect, highly substituted ferrocenes gave lower yields (3r and 3s). However, 1,1′-disubstituted ferrocenes could proceed well (3t and 3u). In terms of metallocenes bearing electron-withdrawing groups, such as acetylferrocene or ferrocenecarboxaldehyde, no desired product could be obtained (see Scheme S1).

Since the protonation of pyridines promoted radical generation, we supposed that the cationization of pyridone could work as well (Figure 2B). 6-Bromo-1-methylpyridin-2(1H)-one was selected to test our assumption. An additive of $Zn(OTf)_2$ improved the yield, probably because its interaction between carbonyl groups made pyridone radical more reactive. After the optimization, the desired C−H heteroarylated product 4a was produced with 60% yield. The molecular structure was confirmed by X-ray analysis. Due to the steric effects, the dihedral angle (41.2°)

Figure 2. Photo-induced C−H heteroarylation of group 8 metallocenes

Condition A: metallocene (0.30 mmol), organic halide (0.20 mmol, X = Br unless otherwise noted), Ir-PC B (3 mol %), TFA (2.0 equiv), NaF (4.0 equiv), TFE (4 mL), under N_2, rt, Kessil LED (390 nm, 40 W), 24 h. Condition B: based on condition A, using $Zn(OTf)_2$ (50 mol %) instead of NaF. Condition C: based on condition A, using TFE/DCM (3 + 1 mL), Kessil LED (427 nm, 40 W) instead of TFE, Kessil LED (390 nm, 40 W). [a]3.0 mmol reaction, Kessil LED (390 nm, 40 W*2), 36 h. [b]Under condition A. [c]Under condition C, using $Zn(OTf)_2$ (50 mol %) instead of NaF. DCM, dichloromethane.

between the Cp and pyridone rings is larger than that of 3a. Substrate with ethyl substituent delivered the corresponding product with a decent yield (4b). With respect to N-hydroxypropyl or benzyl groups, the desired products were obtained with lower yields, probably owing to steric effects (4c–4d). However, the phenethyl group was not applicable to this heteroarylation (4e). When the bromo group substituted at the *para* position, heteroarylation also proceeded to give the desired product (4f). Imidazo[1,2-*a*]pyridines with bromide substituted at *ortho* or *para* positions reacted successfully, providing biheterocyclic products with moderate yields (4g–4h).

Although no pyridylation occurred for some Cp-metal complexes (Ti, Zr, and Mn; Figure 2C), this protocol could be extended to the C−H heteroarylation of ruthenocene (Figure 2D). From the optimization, a mixed solvent of TFE/DCM (3:1, *v/v*) was employed to help the dissolution of ruthenocene. Methyl-substituted pyridines delivered the corresponding products with decent yields (6a and 6b). A medium yield was obtained with 2-bromopyridine (6c). Iodide substituted at the *meta* position also gave the target compound (6d). Notably, when 4-bromo pyridine was used in the reaction, the product was produced with a satisfying yield (6e). With respect to the pyridines-with-protected-amine group, corresponding products were obtained with moderate yields (6f and 6g). A lower yield was observed using the methoxy-group-substituted pyridine (6h). To our delight, useful biheterocyclic products (6i and 6j) could still be obtained in a concise way. The pyridonation of ruthenocene proceeded well to deliver a cross-coupling product (6k), of which the structure was unambiguously confirmed by X-ray analysis.

Mechanistic study

With the intention to understand the mechanism of this photo-induced C−H heteroarylation of metallocenes, preliminary mechanistic experiments were conducted (Figure 3). The addition of butylated hydroxytoluene (BHT) partially decreased the yield of the products (Figure 3A). For 2-bromo-6-methylpyridine 2a, pyridylation preferentially occurred on the phenyl ring of BHT (7a) rather than the hydroxyl group (7a′). When switching to 2-bromopyridine 2b, pyridylation onto the phenyl ring (7b) or the hydroxyl group (7b′) of BHT could both be observed. The addition of the radical scavenger 2,2,6,6-tetramethylpiperidinooxy (TEMPO) completely inhibited the reaction (Figure 3B). These radical trapping experiments indicated a possible radical pathway.

In some cases, ferrocenium ion[61–63] performs as a key intermediate or catalyst during the functionalization of ferrocenes. However, the reaction of ferrocenium hexafluorophosphate under standard conditions delivered only a trace amount of the desired product 3a accompanied with ferrocene 1a (Figure 3C). The addition of extra zinc powder gave the product a decent yield. These two results suggest that *in-situ*-generated electrophilic pyridyl radicals react with 18e ferrocene rather than 17e ferrocenium to form the new C−C bond.

Light-on/-off experiments revealed that consistent irradiation of an LED was essential for this protocol (Figure 3D). Furthermore, the corresponding quantum yield (Φ)[64] has been subsequently determined as 0.65. Afterward, Stern−Volmer quenching experiments of $[Ir(ppy)_2(bim)]PF_6$ with different conditions were conducted (Figure 3E). The addition of pyridine bromide (2a) or TFA individually into the solution of the photocatalyst showed a slight quenching effect. However, the combination of 2a with TFA displayed a dramatic quenching effect even at lower concentrations. This suggests that the protonation of pyridine is essential for a highly efficient single electron transfer (SET) from excited photocatalyst to halopyridine (2a). As described in

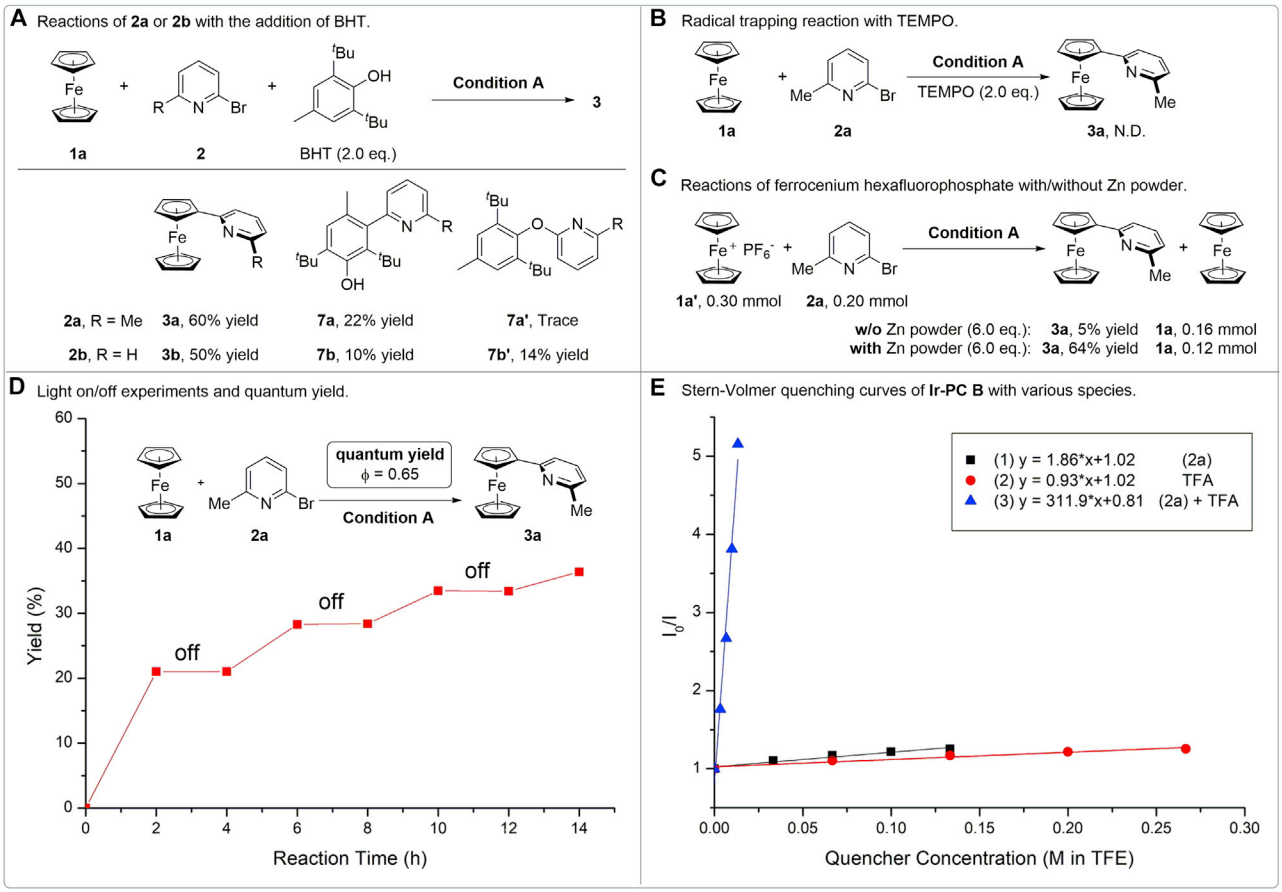

Figure 3. Mechanistic studies
TEMPO, 2,2,6,6-Tetramethylpiperidinooxy.

our previous work,[59] the protonation of halopyridine (2a) probably increases its reduction potential, making it feasible for it to be reduced by the excited state of $[Ir(ppy)_2(bim)]PF_6$.

Based on the experimental results mentioned above and literature reports on photo-induced reactions,[59] a proposed mechanism has been shown in Scheme 1. First, under the irradiation of an LED, the photocatalyst is transformed from the ground state to excited state Ir(III)*. A subsequent SET from Ir(III)* species to protonated halopyridine A generates pyridyl radical B. Then, the pyridyl radical B undergoes an electrophilic radical attack onto 18e ferrocene to give the intermediate C with a newly formed C−C bond. Another SET process from intermediate C to Ir(IV) delivers ferrocenyl pyridinium and regenerates photocatalyst Ir(III) for the next cycle. The desired product 3a could be obtained after a basic work up.

Synthetic transformations

Finally, further transformations of pyridyl ferrocene were conducted to demonstrate the synthetic utility of this protocol (Scheme 2). Taking advantage of inherent DGs of 3a,[65] C−H amination of ferrocene was accomplished with a high yield (8aA, 91%). With the help of Ir catalysis,[66] sp^2 alkenylation on the Cp ring was achieved with 71% yield (8b). A selective sp^3 rather than sp^2 C−H alkylation on the methyl group of pyridines (8c) was facilitated by Pd catalysis.[67] Through a classic electrophilic

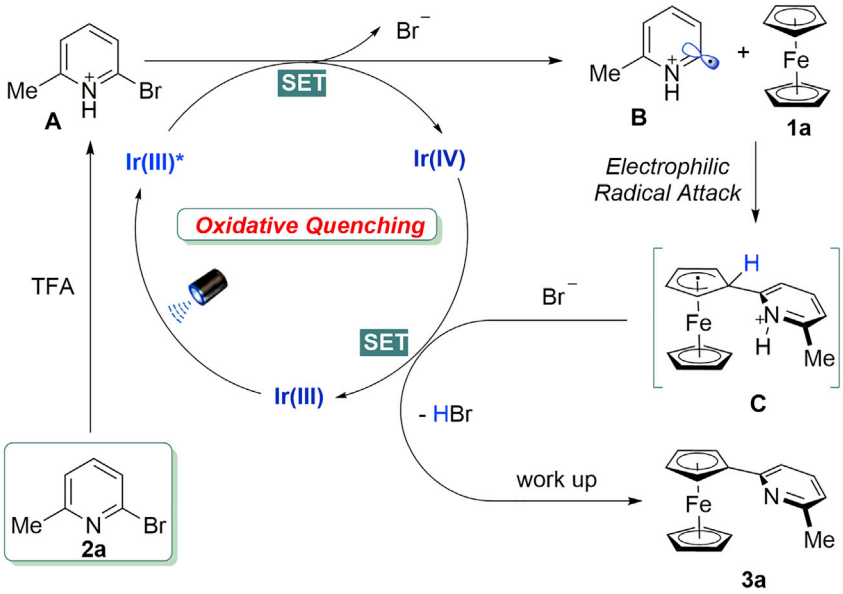

Scheme 1. Proposed mechanism

Friedel-Crafts reaction, a useful acyl group could be introduced onto the other Cp ring of ferrocene 3a with a decent yield (8d, 70%).[22]

In conclusion, we have developed a direct C−H heteroarylation of group 8 metallocenes under photoredox catalysis. A variety of functionalized ferrocenes and ruthenocenes have been easily constructed through this intermolecular cross coupling in the absence of preinstalled DGs. Preliminary mechanistic studies suggest an electrophilic radical substitution of metallocene with heteroaryl radical is involved in the formation of a new C−C bond. Further transformations of pyridyl ferrocene were also demonstrated to show the synthetic utility of this protocol. Overall, this concise and mild strategy may serve as a general complement for accessing synthetically useful heteroarylated metallocenes.

EXPERIMENTAL PROCEDURES

Resource availability

Lead contact

Further information and requests for resources and reagents should be directed to and will be fulfilled by the lead contact, Qing-An Chen (qachen@dicp.ac.cn).

Materials availability

Commercially available reagents were used without further purification. Other solvents were treated prior to use according to the standard methods. Unless otherwise stated, all reactions were conducted under inert atmosphere using standard Schlenk techniques or in a nitrogen-filled glovebox. ^{1}H NMR and ^{13}C NMR spectra were recorded at room temperature in $CDCl_3$ on 400 or 700 MHz instruments with tetramethylsilane (TMS) as the internal standard. Flash column chromatography was performed on silica gel (200–300 mesh). All reactions were monitored by thin-layer chromatography (TLC), nuclear magnetic resonance (NMR), or gas chromatography with flame-ionization detection (GC-FID) analysis. High-resolution mass spectrometry (HRMS) data were obtained with Micromass HPLC-Q-TOF mass spectrometer (electrospray ionization [ESI]) or Agilent 6540 Accurate-MS spectrometer (quadrupole time of flight [Q-TOF]).

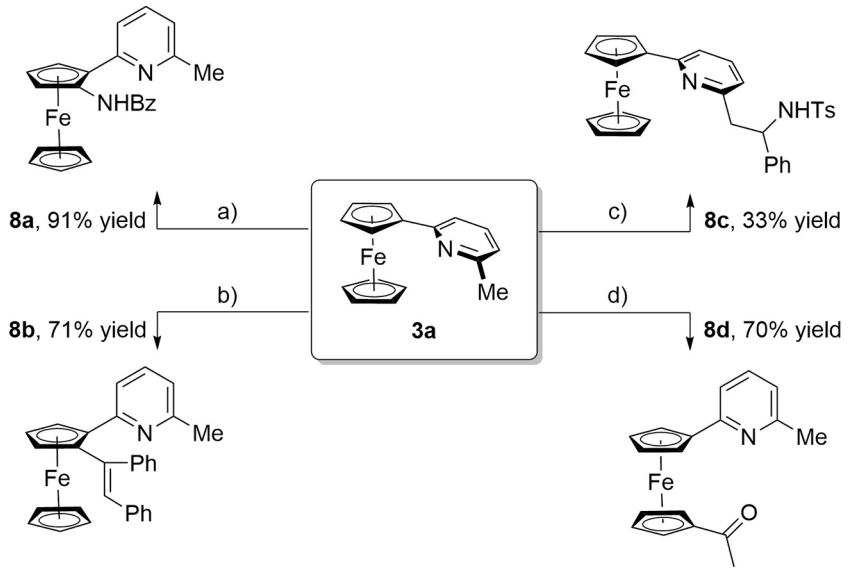

Conditions: a) **3a** (1.0 eq.), 3-phenyl-1,4,2-dioxazol-5-one (1.2 eq.), $[Cp^*RhCl_2]_2$ (2.5 mol%), $AgNTf_2$ (0.15 eq.), NaOAc (0.2 eq.), DCE, 70 °C, 17 h. b) **3a** (1.0 eq.), 1,2-diphenylethyne (4.0 eq.), $[Ir(COD)Cl]_2$ (5.0 mol%), $NaBAr^F$ (10 mol%), toluene, 110 °C, 16 h. c) **3a** (2.5 eq.), (*E*)-*N*-benzylidene-4-methylbenzenesulfonamide (1.0 eq.), $Pd(OAc)_2$ (5.0 mol%), Phen (5.0 mol%), THF, 120 °C, 24 h. d) **3a** (1.0 eq.), acetyl chloride (5.0 eq.), $AlCl_3$ (5.0 eq.), DCM, rt, 2 h. Bz = benzoyl group. Ts = paratoluensulfonyl group.

Scheme 2. Synthetic transformations

Data and code availability

The authors declare that data supporting the findings of this study are available within the article and the Supplemental information. Crystallographic data for the structures reported in this article have been deposited at the Cambridge Crystallographic Data Center (CCDC) under CCDC: 2109760 (3a), 2109766 (4a), and 2112906 (6k). Copies of the data can be obtained free of charge from https://www.ccdc.cam.ac.uk/structures/. All other data are available from the lead contact upon reasonable request.

Description of methods and characterization

Further experimental descriptions, the general information, details of the reagents, and all syntheses and characterizations are provided in the Supplemental experimental procedures. Tables S1–S9 show detailed optimizations for photo-induced C–H heteroarylation of ferrocene and ruthenocene. Scheme S1 shows some unsuccessful substrates. Table S10, Figures S1–S3, and Equations S1–S4 show the details for the determination of the reaction quantum yield. Table S11 and Figure S4 show the details for light-on/-off experiments. Figures S5–S8 show details for the Stern-Volmer experiments. Tables S12–S14 show the crystal data and structures of 3a, 4a, and 6k. NMR spectra are provided in Figures S9–S112.

SUPPLEMENTAL INFORMATION

Supplemental information can be found online at https://doi.org/10.1016/j.xcrp.2022.100768

ACKNOWLEDGMENTS

We thank Prof. Zhi-Shi Ye (DUT) for helpful discussions and manuscript revisions. Financial support from Dalian Outstanding Young Scientific Talent (2020RJ05) and the National Natural Science Foundation of China (22071239) is acknowledged.

AUTHOR CONTRIBUTIONS

Q.-A.C. conceived and supervised the project. Q.-A.C., G.-C.H., and S.-Y.G. designed the experiments. G.-C.H., S.-Y.G., H.Z., C.-H.L., Y.L., X.-T.M., and D.-W.J. performed the experiments and analyzed the data.

DECLARATION OF INTERESTS

The authors declare no competing interests.

Received: December 6, 2021
Revised: January 11, 2022
Accepted: January 21, 2022
Published: February 16, 2022

REFERENCES

1. Hayashi, T., and Togni, A. (1995). Ferrocenes (Wiley-VCH).
2. Togni, A., and Haltermann, R.L. (1998). Metallocenes (Wiley-VCH).
3. Štěpnička, P. (2008). Ferrocenes (Wiley-VCH).
4. Moriuchi, T., and Hirao, T. (2010). Design of ferrocene-dipeptide bioorganometallic conjugates to induce chirality-organized structures. Acc. Chem. Res. *43*, 1040–1051.
5. Quintana, M., Vazquez, E., and Prato, M. (2013). Organic functionalization of graphene in dispersions. Acc. Chem. Res. *46*, 138–148.
6. Wu, L.Z., Chen, B., Li, Z.J., and Tung, C.H. (2014). Enhancement of the efficiency of photocatalytic reduction of protons to hydrogen via molecular assembly. Acc. Chem. Res. *47*, 2177–2185.
7. Wei, J., and Diaconescu, P.L. (2019). Redox-switchable ring-opening polymerization with ferrocene derivatives. Acc. Chem. Res. *52*, 415–424.
8. Jaouen, G., Vessieres, A., and Top, S. (2015). Ferrocifen type anti cancer drugs. Chem. Soc. Rev. *44*, 8802–8817.
9. Albada, B., and Metzler-Nolte, N. (2016). Organometallic-peptide bioconjugates: synthetic strategies and medicinal applications. Chem. Rev. *116*, 11797–11839.
10. Vessières, A., Wang, Y., McGlinchey, M.J., and Jaouen, G. (2021). Multifaceted chemical behaviour of metallocene (M = Fe, Os) quinone methides. Their contribution to biology. Coord. Chem. Rev. *430*, 213658.
11. Dai, L.X., and Hou, X.L. (2010). Chiral Ferrocenes in Asymmetric Catalysis (Wiley-VCH).
12. Dai, L.X., Tu, T., You, S.L., Deng, W.P., and Hou, X.L. (2003). Asymmetric catalysis with chiral ferrocene ligands. Acc. Chem. Res. *36*, 659–667.
13. Atkinson, R.C., Gibson, V.C., and Long, N.J. (2004). The syntheses and catalytic applications of unsymmetrical ferrocene ligands. Chem. Soc. Rev. *33*, 313–328.
14. Fu, G.C. (2004). Asymmetric catalysis with "planar-chiral" derivatives of 4-(dimethylamino) pyridine. Acc. Chem. Res. *37*, 542–547.
15. Gomez Arrayas, R., Adrio, J., and Carretero, J.C. (2006). Recent applications of chiral ferrocene ligands in asymmetric catalysis. Angew. Chem. Int. Ed. Engl. *45*, 7674–7715.
16. Zhu, D.-Y., Chen, P., and Xia, J.-B. (2016). Synthesis of planar chiral ferrocenes by transition-metal-catalyzed enantioselective C−H activation. ChemCatChem. *8*, 68–73.
17. Gao, D.W., Gu, Q., Zheng, C., and You, S.L. (2017). Synthesis of planar chiral ferrocenes via transition-metal-catalyzed direct C-H bond functionalization. Acc. Chem. Res. *50*, 351–365.
18. Liu, C.-X., Gu, Q., and You, S.-L. (2020). Asymmetric C–H bond functionalization of ferrocenes: new opportunities and challenges. Trends Chem. *2*, 737–749.
19. Shibata, T., and Shizuno, T. (2014). Iridium-catalyzed enantioselective C-H alkylation of ferrocenes with alkenes using chiral diene ligands. Angew. Chem. Int. Ed. Engl. *53*, 5410–5413.
20. Lou, S.J., Zhuo, Q., Nishiura, M., Luo, G., and Hou, Z. (2021). Enantioselective C-H alkenylation of ferrocenes with alkynes by half-sandwich scandium catalyst. J. Am. Chem. Soc. *143*, 2470–2476.
21. Sünkel, K., and Weigand, S. (2011). 2-Pyridylmetallocenes: part I. electrophilic halogenation of 2-pyridylferrocene. Molecular structures of 2-pyridylferrocene and its α-brominated and -fluorinated derivatives. Synthesis of 2-pyridylruthenocene and 2-pyridylcymantrene. Inorg. Chim. Acta *370*, 224–229.
22. Gao, D.W., Yin, Q., Gu, Q., and You, S.L. (2014). Enantioselective synthesis of planar chiral ferrocenes via Pd(0)-catalyzed intramolecular direct C-H bond arylation. J. Am. Chem. Soc. *136*, 4841–4844.
23. Deng, R., Huang, Y., Ma, X., Li, G., Zhu, R., Wang, B., Kang, Y.B., and Gu, Z. (2014). Palladium-catalyzed intramolecular asymmetric C-H functionalization/cyclization reaction of metallocenes: an efficient approach toward the synthesis of planar chiral metallocene compounds. J. Am. Chem. Soc. *136*, 4472–4475.
24. Cai, Z.J., Liu, C.X., Wang, Q., Gu, Q., and You, S.L. (2019). Thioketone-directed rhodium(I) catalyzed enantioselective C-H bond arylation of ferrocenes. Nat. Commun. *10*, 4168.
25. Liu, C.X., Cai, Z.J., Wang, Q., Wu, Z.J., Gu, Q., and You, S.L. (2020). Rhodium-catalyzed pyridine-assisted C–H arylation for the synthesis of planar chiral ferrocenes. CCS Chem. *2*, 642–651.
26. Narayanam, J.M.R., and Stephenson, C.R.J. (2011). Visible light photoredox catalysis: applications in organic synthesis. Chem. Soc. Rev. *40*, 102–113.
27. Prier, C.K., Rankic, D.A., and MacMillan, D.W. (2013). Visible light photoredox catalysis with transition metal complexes: applications in organic synthesis. Chem. Rev. *113*, 5322–5363.
28. Gentry, E.C., and Knowles, R.R. (2016). Synthetic applications of proton-coupled electron transfer. Acc. Chem. Res. *49*, 1546–1556.
29. Hopkinson, M.N., Tlahuext-Aca, A., and Glorius, F. (2016). Merging visible light photoredox and gold catalysis. Acc. Chem. Res. *49*, 2261–2272.
30. Romero, N.A., and Nicewicz, D.A. (2016). Organic photoredox catalysis. Chem. Rev. *116*, 10075–10166.

31. Skubi, K.L., Blum, T.R., and Yoon, T.P. (2016). Dual catalysis strategies in photochemical synthesis. Chem. Rev. *116*, 10035–10074.

32. Tellis, J.C., Kelly, C.B., Primer, D.N., Jouffroy, M., Patel, N.R., and Molander, G.A. (2016). Single-electron transmetalation via photoredox/nickel dual catalysis: unlocking a new paradigm for sp(3)-sp(2) cross-coupling. Acc. Chem. Res. *49*, 1429–1439.

33. Chen, Y., Lu, L.-Q., Yu, D.-G., Zhu, C.-J., and Xiao, W.-J. (2018). Visible light-driven organic photochemical synthesis in China. Sci. China Chem. *62*, 24–57.

34. Wang, C.S., Dixneuf, P.H., and Soule, J.F. (2018). Photoredox catalysis for building C-C bonds from C(sp(2))-H Bonds. Chem. Rev. *118*, 7532–7585.

35. Cybularczyk-Cecotka, M., Szczepanik, J., and Giedyk, M. (2020). Photocatalytic strategies for the activation of organic chlorides. Nat. Catal. *3*, 872–886.

36. Zhu, C., Yue, H., Chu, L., and Rueping, M. (2020). Recent advances in photoredox and nickel dual-catalyzed cascade reactions: pushing the boundaries of complexity. Chem. Sci. *11*, 4051–4064.

37. Witzel, S., Hashmi, A.S.K., and Xie, J. (2021). Light in gold catalysis. Chem. Rev. *121*, 8868–8925.

38. Zhu, C., Yue, H., Jia, J., and Rueping, M. (2021). Nickel-catalyzed c-heteroatom cross-coupling reactions under mild conditions via facilitated reductive elimination. Angew. Chem. Int. Ed. Engl. *60*, 17810–17831.

39. Bobo, M.V., Kuchta, J.J., III, and Vannucci, A.K. (2021). Recent advancements in the development of molecular organic photocatalysts. Org. Biomol. Chem. *19*, 4816–4834.

40. Felpin, F.X., and Sengupta, S. (2019). Biaryl synthesis with arenediazonium salts: cross-coupling, CH-arylation and annulation reactions. Chem. Soc. Rev. *48*, 1150–1193.

41. Li, H., Tang, X., Pang, J.H., Wu, X., Yeow, E.K.L., Wu, J., and Chiba, S. (2021). Polysulfide anions as visible light photoredox catalysts for aryl cross-couplings. J. Am. Chem. Soc. *143*, 481–487.

42. Zoller, J., Fabry, D.C., and Rueping, M. (2015). Unexpected dual role of titanium dioxide in the visible light heterogeneous catalyzed C–H arylation of heteroarenes. ACS Catal. *5*, 3900–3904.

43. Tobisu, M., Furukawa, T., and Chatani, N. (2013). Visible light-mediated direct arylation of arenes and heteroarenes using diaryliodonium salts in the presence and absence of a photocatalyst. Chem. Lett. *42*, 1203–1205.

44. Bobo, M.V., Arcidiacono, A.M., Ayare, P.J., Reed, J.C., Helton, M.R., Ngo, T., and Vannucci, A.K. (2020). A series of green light absorbing organic photosensitizers capable of oxidative quenching photocatalysis. ChemPhotoChem *5*, 51–57.

45. Cheng, Y., Gu, X., and Li, P. (2013). Visible-light photoredox in homolytic aromatic substitution: direct arylation of arenes with aryl halides. Org. Lett. *15*, 2664–2667.

46. Ghosh, I., Ghosh, T., Bardagi, J.I., and Konig, B. (2014). Reduction of aryl halides by consecutive visible light-induced electron transfer processes. Science *346*, 725–728.

47. Ghosh, I., Shaikh, R., and Konig, B. (2017). Sensitization-initiated electron transfer for photoredox catalysis. Angew. Chem. Int. Ed. Engl. *56*, 8544–8549.

48. Bartolomeu, A.A., Silva, R.C., Brocksom, T.J., Noel, T., and de Oliveira, K.T. (2019). Photoarylation of pyridines using aryldiazonium salts and visible light: an EDA approach. J. Org. Chem. *84*, 10459–10471.

49. Huang, G., Li, B., Liu, W., Shi, L., and Ma, Y. (2000). Facile and effective preparation of substituted phenylferrocene under phase transfer catalysis. J. Chem. Res. *2000*, 491–492.

50. Aycock, R.A., Wang, H., and Jui, N.T. (2017). A mild catalytic system for radical conjugate addition of nitrogen heterocycles. Chem. Sci. *8*, 3121–3125.

51. Chen, D., Xu, L., Long, T., Zhu, S., Yang, J., and Chu, L. (2018). Metal-free, intermolecular carbopyridylation of alkenes via visible-light-induced reductive radical coupling. Chem. Sci. *9*, 9012–9017.

52. Seath, C.P., Vogt, D.B., Xu, Z., Boyington, A.J., and Jui, N.T. (2018). Radical hydroarylation of functionalized olefins and mechanistic investigation of photocatalytic pyridyl radical reactions. J. Am. Chem. Soc. *140*, 15525–15534.

53. Zhu, S., Qin, J., Wang, F., Li, H., and Chu, L. (2019). Photoredox-catalyzed branch-selective pyridylation of alkenes for the expedient synthesis of Triprolidine. Nat. Commun. *10*, 749.

54. Jung, S., Shin, S., Park, S., and Hong, S. (2020). Visible-light-driven c4-selective alkylation of pyridinium derivatives with alkyl bromides. J. Am. Chem. Soc. *142*, 11370–11375.

55. Lee, K., Lee, S., Kim, N., Kim, S., and Hong, S. (2020). Visible-light-enabled trifluoromethylative pyridylation of alkenes from pyridines and triflic anhydride. Angew. Chem. Int. Ed. Engl. *59*, 13379–13384.

56. Moon, Y., Lee, W., and Hong, S. (2020). Visible-light-enabled ortho-selective aminopyridylation of alkenes with N-aminopyridinium ylides. J. Am. Chem. Soc. *142*, 12420–12429.

57. Min, X.T., Ji, D.W., Guan, Y.Q., Guo, S.Y., Hu, Y.C., Wan, B., and Chen, Q.A. (2020). Visible light induced bifunctional rhodium catalysis for decarbonylative coupling of imides with alkynes. Angew. Chem. Int. Ed. Engl. *60*, 1583–1587.

58. Guan, Y.Q., Min, X.T., He, G.C., Ji, D.W., Guo, S.Y., Hu, Y.C., and Chen, Q.A. (2021). The serendipitous effect of KF in Ritter reaction: photo-induced amino-alkylation of alkenes. iScience *24*, 102969–102998.

59. Guo, S.Y., Yang, F., Song, T.T., Guan, Y.Q., Min, X.T., Ji, D.W., Hu, Y.C., and Chen, Q.A. (2021). Photo-induced catalytic halopyridylation of alkenes. Nat. Commun. *12*, 6538.

60. Garra, P., Damien, B., Guillaume, N., Bernadette, G., Fabrice, M.-S., Céline, D., Valery, F.S., Frédéric, D., David, D., Didier, G., et al. (2019). Ferrocene-based (photo)redox polymerization under long wavelengths. Polym. Chem. *10*, 1431–1441.

61. Foo, K., Sella, E., Thome, I., Eastgate, M.D., and Baran, P.S. (2014). A mild, ferrocene-catalyzed C-H imidation of (hetero)arenes. J. Am. Chem. Soc. *136*, 5279–5282.

62. Walawalkar, M.G., Pandey, P., and Murugavel, R. (2021). The redox journey of iconic ferrocene: ferrocenium dications and ferrocenate anions. Angew. Chem. Int. Ed. Engl. *60*, 12632–12635.

63. Walker, B.R., Manabe, S., Brusoe, A.T., and Sevov, C.S. (2021). Mediator-enabled electrocatalysis with ligandless copper for anaerobic chan-lam coupling reactions. J. Am. Chem. Soc. *143*, 6257–6265.

64. Cismesia, M.A., and Yoon, T.P. (2015). Characterizing chain processes in visible light photoredox catalysis. Chem. Sci. *6*, 5426–5434.

65. Wang, S.-B., Gu, Q., and You, S.-L. (2017). Cp*Rh(III)-Catalyzed C–H amidation of ferrocenes. Organometallics *36*, 4359–4362.

66. Takebayashi, S., and Shibata, T. (2012). $[Ir(cod)_2]$BARF-catalyzed C–H bond alkenylation and alkylation of ferrocenes. Organometallics *31*, 4114–4117.

67. Qian, B., Guo, S., Shao, J., Zhu, Q., Yang, L., Xia, C., and Huang, H. (2010). Palladium-catalyzed benzylic addition of 2-methyl azaarenes to N-sulfonyl aldimines via C-H bond activation. J. Am. Chem. Soc. *132*, 3650–3651.